
Article:
Mármol, G., Savastano, H., Tashima, M.M. et al. (1 more author) (2016) Optimization of the MgO-SiO₂ binding system for fiber-cement production with cellulosic reinforcing elements. Materials & Design, 105. pp. 251-261. ISSN 0261-3069

https://doi.org/10.1016/j.matdes.2016.05.064

This is a preprint version of an article published in Materials & Design. The version of record is available at http://dx.doi.org/10.1016/j.matdes.2016.05.064

Optimization of the $MgO\text{-}SiO_2$ binding system for fiber-cement production with cellulosic reinforcing elements.

Gonzalo Mármol [a], Holmer Savastano Jr [a], Mauro M. Tashima [b], John L. Provis [c]

[a] University of São Paulo – Faculty of Animal Science and Food Engineering, Department of Biosystems Engineering, Duque de Caxias Norte Street, 225, 13630-000 Pirassununga, SP, Brazil

[b] UNESP – Universidade Estadual Paulista, Campus de Ilha Solteira, Alameda Bahia, 550, 15385-000 Ilha Solteira, SP, Brazil

[c] Department of Materials Science and Engineering, University of Sheffield, Sir Robert Hadfield Building, Mappin St, Sheffield S1 3JD, UK

Corresponding author:

Gonzalo Mármol, **e-mail:**gonzalo.marmol@usp.br

ABSTRACT

A range of MgO and SiO_2 blends mixed with water are analyzed to develop clinker-free fiber-cement products reinforced with cellulosic fibers. The target is the development of a binder which is not chemically aggressive to the fibers, but which develops high mechanical strength Mechanical performance of the materials developed is not only influenced by magnesium silicate hydrate (M-S-H) gel content, but is more related to the void content within the paste due to unreacted water, meaning that the gel-space ratio concept is valuable in describing the compressive strengths of these materials. A higher MgO content in the mix formulation leads to M-S-H gels with increased Mg/Si ratio. The Mg/Si ratio also increases over time for each mix, indicated by changes in the gel structure as reaction is not yet complete after 28 days. SEM shows a heterogeneous microstructure which also has regions of high Si content. The 60wt.%MgO-40wt.%SiO_2 system is chosen as the optimal formulation since it is the least alkaline binder with high mechanical strength. Bending tests on pastes reinforced with cellulosic pulps prove the efficiency of this binder, which preserves the reinforcing capacity of the fibers much better than Portland cement pastes after 200 cycles of accelerated ageing.

Keywords: Magnesia-silica fiber-cement; compressive strength; X-ray diffraction; SEM; cellulose conservation

1. INTRODUCTION

Lignocellulosic fibers have increasingly become a very interesting material as a reinforcement element for fiber-cement products, e.g. flat sheets, roofing and siding shingles, and clapboards, due to their excellent mechanical properties [1]. Many other types of fibers present a remarkable potential as reinforcement in cementitious products, e.g. carbon [2,3], synthetic polymers [4], rubber [5], glass fiber reinforced plastic [6] or steel [7,8], although each has either economic and environmental disadvantages compared to cellulosic fibers. However, when used with Portland cement, this type of fibers undergoes alkaline degradation, leading to deterioration in flexural properties over time. Two main fibre degradation mechanisms have been reported for cellulosic fibers used to reinforce cementitious composites: fibre mineralization due to the precipitation of calcium hydroxide in the fibre cells and surface, and degradation of cellulose, hemicellulose and lignin due to the adsorption of calcium and hydroxyl ions [9–11]. Vegetable fibers can suffer various degrees of degradation when exposed to an alkaline environment, and this degradation is especially manifested when the alkaline environments are also rich in Ca^{2+} [12].

Many attempts to solve this inconvenience have been explored effectively, improving fiber integrity after ageing, although far from achieving a completely successful solution. So far, all the techniques used to improve vegetable fiber durability in Portland cement are based on the reduction of portlandite content in the binder, by the use of highly reactive pozzolans [13–15] or by carbonation [16–18]. However, these methods rely on chemical reactions which take place in the binder gradually rather than immediately, and this means that the vegetable fibers are surrounded by high concentrations of $Ca(OH)_2$ in the initial stages of hardening, which may be deleterious for reinforcing performance [12].

A different solution becomes possible where Ca chemistry is replaced by Mg, and the cement is produced by combining reactive MgO and highly reactive amorphous SiO_2 to form magnesium silicate hydrate (M-S-H in cement chemistry nomenclature, M: MgO; S: SiO_2; H: H_2O) [19]. In initial studies of this system, a high content of bonding M-S-H was achieved with satisfactory mechanical properties [19]. Whereas this type of cement historically attracted limited interest, during the last decade it has become an attractive alternative to Portland cement in specific applications, such as this, due to its low alkalinity (pH < 11) [20,21] and potentially good mechanical performance [22,23].

In the particular case of fiber-cement production it is especially necessary to understand the early-age properties of the binding matrix, since rapid development of rigidity (in the first week of aging) is required. For this reason, this paper assesses the evolution of hydration from 7 to 28 days of different MgO-SiO_2 formulations, simulating the fiber-cement manufacture conditions, selecting the optimal dosage as a compromise solution between the lowest alkalinity (from mixing until 28 days) and the highest mechanical performance (at 7 and 28 days).

The better understanding of this new fiber-cement product is crucial for the manufacture of more sustainable building materials, since cellulosic fibers are biodegradable, renewable, demand low processing energy, and are available around the world at low cost, with a diversity of morphologies and dimensions [24]. In addition, MgO-SiO_2 cements, in contrast to Portland cement which requires high temperatures (about 1450°C) during production, demand less energy (750°C to obtain reactive MgO from magnesium carbonate [25]) and also allows the reuse of agro-industrial residues to obtain amorphous silica [26], thus becoming a more efficient cement from an environmental point of view.

2. MATERIALS AND METHODS

This work is structured in two stages. The first stage aims to analyze MgO-SiO_2 systems with different formulations, and particularly their hydration reactions in the early stages. The second stage involves selection of the optimal blended system for fiber-cement production according to the assessment of pH and mechanical performance, and testing its effectiveness to avoid damage to cellulosic reinforcement elements by 4-point bending tests at 28 days and after accelerated ageing.

2.1 Raw materials

Pastes made of a mixture of fine powders acted as clinker-free cement. The two components of this blended cement were high surface area reactive magnesium oxide powder, Q-MAG-200-AR (AR200), obtained by controlled calcination of magnesite (natural magnesium carbonate) and provided by Magnesita S.A., Contagem, MG, Brazil, and undensified microsilica powder type 920U with a typical bulk density of 200-350 kg/m^3, provided by Elkem ASA Materials, Sao Paulo, SP, Brazil. Dry ball milling for powder homogenization in steel chamber with steel balls (ASTECMA, Brazil) was carried out at a ball:powder ratio of 2:1 at 1 rpm for 30 min. The basic properties of these materials are shown in Table 1.

Table 1- Properties of the raw materials used to produce the blended samples. LOI is loss on ignition at 1000°C.

	MgO AR200	SiO_2 920U
	Chemical composition by XRF (wt.%)	
MgO	97.4	0.33
SiO_2	0.1	95.1
Al_2O_3	<0.10	<0.10
Fe_2O_3	0.34	0.35
CaO	0.81	0.25
TiO_2	<0.10	<0.10
K_2O	<0.10	0.91
Na_2O	<0.10	0.26
LOI	1.6	1.7
	Particle density (g/cm^3)	
	3.5	2.3
	Particle size distribution	
D_{10} (μm)	7.1	11.4
D_{50} (μm)	17.4	19.0
D_{90} (μm)	64.6	37.0
	Surface area by BET method(m^2/g)	
	22.7	16.1

The initial MgO to SiO_2 ratios of the cements were defined according to Table 2. For every sample, including Portland cement pastes, the water to binder ratio was held constant at 0.50 in order to compare mechanical results regardless of the water demand of the powders. For

that purpose, plasticizer (Melflux 2651F provided by Sika) was added to the samples for binary systems.

Table 2- Compositions of the blends of MgO and SiO_2 analyzed

MgO (wt.%)	SiO_2 (wt.%)
50	50
60	40
70	30
80	20

2.2 Analytical techniques

Analysis by X-ray diffraction (XRD) was carried out using powder samples, using an X-ray diffractometer Horiba LA-960, with CuKα radiation generated at a voltage of 40 kV and a current of 30 mA, and scanning between 5-65° 2θ at 10 °/min. Rietveld analysis was performed using PDXL-2 software; samples made of 100% AR200 MgO, both hydrated and non hydrated, were used to refine and calibrate the parameters of the XRD peaks in systems with MgO and $Mg(OH)_2$. Lattice constants were a=b=c=4.2124 Å and $\alpha=\beta=\gamma=90^o$ for periclase; and a=b=3.14569 Å, c=4.7735 Å and $\alpha=\beta=90^o$ and $\gamma=120^o$ for brucite. Pseudo-Voigt peak shapes were used in all refinements. Before analyzing the intensities of brucite and periclase, the displayed bumps corresponding to unreacted silica and M-S-H (based on the literature,[27,28]) were decomposed by multiple peak separation (pseudo-Voigt shaped) and their intensities were also calculated to avoid overlap with crystalline phases. Fig. 1a shows schematic observed and calculated XRD diffractograms of the MgO-SiO_2 paste, with the different peaks and bumps used for the phase quantification, and a residual curve illustrating an excellent fit to the data. Peaks obtained from impurities were neglected for crystalline phase determination.

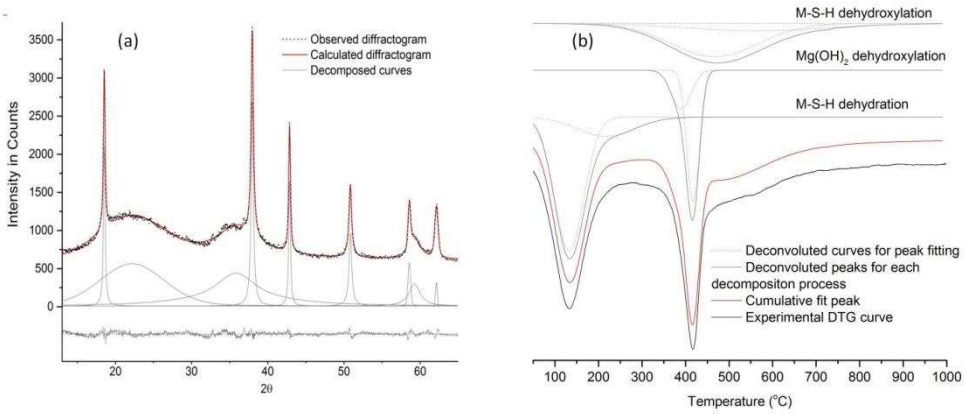

Fig. 1- (a) Observed and calculated XRD diffractograms for MgO and $Mg(OH)_2$ quantification, with the different decomposed curves matching the corresponding phases and a residual curve, and (b) DTG curve deconvolution for mass loss quantification of each decomposition process for one of the MgO-SiO_2 pastes studied.

Thermogravimetry tests were conducted using a Netzch STA 440 F3 Jupiter instrument under an atmosphere of nitrogen set at a flow rate of 60 mL/min, from 25 to 1000 ^{o}C at a heating rate of 10 ^{o}C/min. Deconvolution of the first derivative TG (DTG) curves was undertaken using a combination of Gauss and Lorentz curves to quantify the mass loss corresponding to each different stage of dehydration/dehydroxylation (Fig. 1b). In order aid in characterization of the expected M-S-H gels in the cements produced, a synthetic gel with a Mg/Si molar ratio of 0.50 was also produced via a precipitation method according to prior work [23,29] using solutions of sodium metasilicate pentahydrate ($Na_2SiO_3 \cdot 5H_2O$) and magnesium nitrate hexahydrate ($Mg(NO_3)_2 \cdot 6H_2O$). This gel was used as a thermogravimetric reference, with a low Mg content to avoid $Mg(OH)_2$ contamination via the presence of excess Mg during the precipitation synthesis.

For infrared spectroscopy, attenuated total reflection (ATR) tests were carried out with a NEXUS 670 spectrometer from Nicolet Instrument Corporation, observing wavenumbers between 4000 and 400 cm^{-1}. Scanning electron microscopy (SEM) images were collected with a Hitachi TM3000 microscope, and EDS measurements were conducted with a SwiftED3000, Oxford Instruments. The acceleration voltage used for the SEM analysis was 15 kV.

2.3 Selection of the optimal binder matrix

The evolution of pH over time in MgO-SiO_2 slurries representing the cement samples was measured following the procedures of previous studies [20]. 10 g of blended powders, in ratios according to Table 2, were poured into sealed glass beakers containing 100 mL of deionized water, and stirred. The temperature was kept constant at 30 ^{o}C. pH measurements were taken 30 min after mixing the powders in water, then at 1, 7, 14, 21 and 28 days. For pH measurements a Digimed DM-23 pH-meter, an Ika HS10 magnetic stirrer and an Ika ETS-D5 digital temperature controller were used.

One of the key criteria used to select the best formulation was mechanical performance. Although the final target of this work is a fiber-reinforced product with good flexural strength, , the value that represents the performance of the cement paste itself in a more reliable manner is compressive strength. An adaptation of standardized mortar tests (ASTM C780-14, 2014) for application to pastes was selected in order to use materials in a more efficient way as a lower amount of material was required to achieve consistent results. Axial compressive

strength was measured at 7 and 28 days (6 replicate cylindrical test samples, 50 mm high x 25 mm diameter, per curing time), performing the test with a 50 kN cell load and a swivel device to enable a uniform approach to the upper side of the samples. The deformation rate was 0.3 mm/min. The samples were cured in a sealed bag and kept in a 95% humidity chamber. After compressive strength testing, samples were crushed into powder and immersed in acetone for 5 days and then dried at 65 ^{o}C until constant mass, for further analysis.

2.4 Flexural characterization of fiber-cement elements reinforced with cellulosic pulp

The fiber-cement composites were made out of 95 wt.% cement paste and 5 wt.% of unbleached pulp, characterized according to [30]. Flat pads with a thickness of around 6 mm were produced at laboratory scale using a slurry vacuum-dewatering process followed by a pressing technique, as described in detail by Savastano et al. [31], and were wet cut into four 165 mm × 40 mm flexural test specimens. Mechanical tests were performed at 28 days, and after 200 cycles of accelerated ageing (as described below), using a testing machine EMIC DL 3000 equipped with 1 kN load cell and a deflectometer. The deflection values were divided by the major span (135 mm) of the bending test, and considered as specific deflection (ε). A four-point bending configuration [14] was employed to determine Modulus of Rupture (MOR) and Specific Deflection at MOR. MOR was calculated as: $MOR = \frac{P_{máx} \cdot L}{b \cdot h^2}$.

Accelerated aging cycles were used to speed up natural weathering using soaking and drying cycles, to provide a better understanding of the long-term behavior of the composites. Specimens were successively immersed into water at 20±5^{o}C for 170 min and then, after an interval of 10 min, heated to 60±5^{o}C for 170 min in a ventilated oven. Another interval of 10 min at room temperature also preceded the subsequent cycle, as recommended by the standard EN 494:2012 [32]. Each cycle was defined as one soak and dry, and the samples were submitted to 200 accelerated aging cycles.

As a control cement matrix, High Early Strength Portland Cement was used (CPV-ARI, according to Brazilian Standards NBR 5733) to compare the pH and compressive strength results. CPV-ARI was selected because it is mainly constituted of clinker with no mineral additions. This condition is desirable to set a baseline for the comparative tests here, since mineral additions may induce a pozzolanic reaction, generating a less aggressive environment for lignocellulosic fibers due to the reduction of the portlandite and pH.

3. RESULTS

3.1 XRD characterization

In Fig. 2, XRD patterns for all the samples are depicted. For every sample, it can be seen that peaks corresponding to brucite (at 18.53, 37.96, 50.84 and 58.57 2θ in Table 3) have a higher intensity when compared to peaks matching reflections of periclase (at 42.86 and 61.13 2θ in Table 1). This implies that most of the MgO has either been hydrated to form $Mg(OH)_2$ or reacted to form M-S-H, with a hydration degree close to completion (up to 98% for samples with lower MgO content by QXRD). As expected, formulations with higher contents of MgO show more intense peaks corresponding to both periclase and brucite, as there is less opportunity for conversion to M-S-H in these instances, and thus a lower degree of reaction. The most remarkable difference between samples at 7 and 28 days is that the peak intensities corresponding to periclase decrease with time for every system (Table 3). According to the literature [20,23,29,33–36,28,37,38,27], magnesium silicate hydrate formed by hydration of a mixture of MgO and silica rich powder shows highly disordered characteristics, with broad peaks throughout the diffraction pattern. Two minor, broad peaks are evident here at 33–39° and 58–61° 2θ, centered at 35.8 and 59.3 2θ (Table 3). The other expected broad peak corresponding to magnesium silicate hydrate is supposed to appear between 25-30° 2θ, but in this case it overlaps with the broad feature due to unreacted silica. These features confirm the presence of M-S-H gels [21,23,29,33,34,36,28,37,38,27].

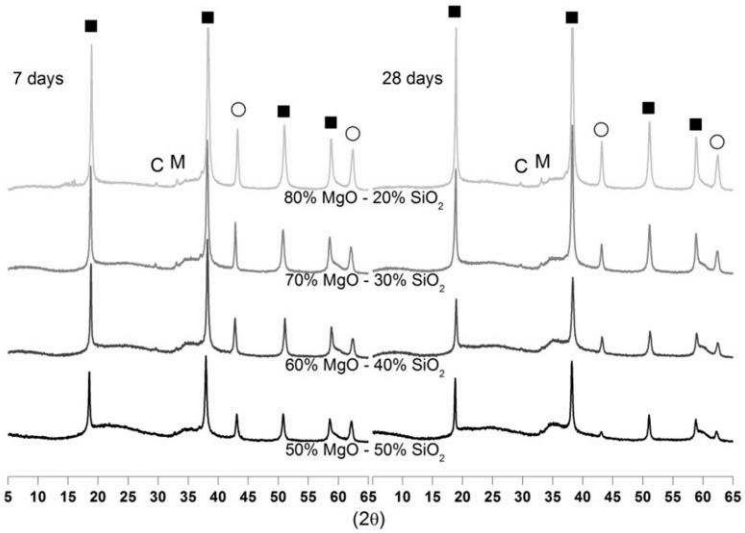

Fig. 2- XRD diffractograms of the different MgO-SiO_2 samples at 7 days (left) and at 28 days (right). Peaks marked are brucite (■), periclase (○), calcite (C) and magnesite (M).

Fig. 3 shows an enlarged view of selected key regions of Fig. 2 for every formulation. Parts of the regions where features arising from M-S-H gel are expected have been omitted since they

overlapped with unreacted silica, brucite and periclase peaks, so Fig. 3 illustrates just the regions where only gel bumps are manifested (33-37° and 59.5-61.5° 2θ). Both regions show a broad hump corresponding to the M-S-H gel XRD patterns obtained in previous studies, confirming the presence of the gel. Nevertheless the intensity of these humps is not as high as it was found in previous works. This may be explained by the fact that M-S-H gel is not the only phase present in the matrix, in contrast to what was intended in previous reports where synthesized magnesium silicate was the only constituent [23,29,35]. In the two regions, between 35-39° and 58-61° 2θ, the intensity of the humps for most of the formulations is slightly higher for 28 day cured samples, suggesting that the development of the gel has been ongoing over time.

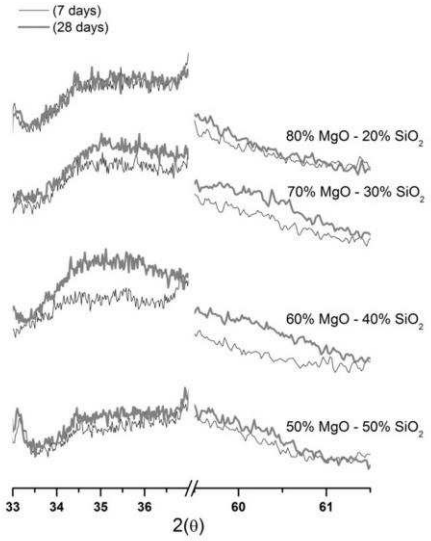

Fig. 3- Enlarged view of the XRD spectra of the regions where gel bumps are present.

Table 3- Peak heights (maximum counts·2θ) of each peak in the XRD diffractograms at 7 and 28 days. The quantification of the crystalline phases (periclase and brucite) was made after subtraction of the amorphous phases (unreacted silica and M-S-H gels) to avoid phase overlapping and impurities.

	50%MgO-50%SiO_2		60%MgO-40%SiO_2		70%MgO-30%SiO_2		80%MgO-20%SiO_2	
Peak center (2θ)	7 days	28 days	7 days	28 days	7 days	28 days	7 days	28 days
18.53	853	694	1114	923	1537	1772	2094	2217
22.17	6336	7447	3259	5774	5347	5822	5925	4771
35.83	5273	5042	7172	4941	5301	5377	2758	3484
37.96	1486	1111	1964	1427	2422	2754	3680	3899
42.86	682	194	443	382	701	504	1062	856
50.84	651	486	851	630	1145	1197	1686	1702
58.57	270	356	442	304	921	810	1124	1203
59.27	787	900	923	1049	557	791	409	389
62.13	479	198	458	355	729	609	1090	963
R^2	0,993	0,974	0,989	0,979	0,986	0,988	0,995	0,993
$Mg(OH)_2$ (wt. %)	19.38	16.11	26.29	20.80	32.29	33.27	43.29	46.30
MgO (wt. %)	6.90	2.38	5.42	4.67	7.66	5.67	10.85	9.33

According to the literature, $Mg(OH)_2$ content tends to decrease with time, although there is little systematic variation observed here due to the replenishment of $Mg(OH)_2$ by ongoing hydration of remnant MgO (Table 3). It is thus evident that $Mg(OH)_2$ reacts with SiO_2 to form more gel [19,21,23,36,28,37,38,27,39]. This phenomenon may be accelerated by pretreatment of the MgO-SiO_2 powdered mixture, either mechanical (grinding) or chemical (use of deflocculants such as sodium phosphates), that can contribute to the reduction of the degree of crystallinity of the $Mg(OH)_2$ formed, and therefore improve defloculation in aqueous environments [40].

3.2 TG characterization

Fig. 4 shows thermogravimetric curves for hydrated MgO and synthetic M-S-H gel at 28 days and their differential curves. From the differential thermogravimetric (DTG) curves two endothermic peaks are visible, one below 300°C corresponding to the synthesized M-S-H gel, and the other corresponding to $Mg(OH)_2$ between ~330 and 460°C [21,23,28,37,38]. These two peaks occur at the same temperatures as the peaks identified in TG analysis of calcium silicate hydrate and calcium hydroxide, the main products obtained during the hydration of tricalcium silicate (C_3S) and dicalcium silicate (C_2S), which together make up 75–80% of Portland cement [41]. From Fig. 4 it is also possible to identify another tiny mass loss peak at around 750°C, which is related to minor atmospheric carbonation of the samples.

Fig. 5 displays TG and DTG analysis for all formulations containing MgO and SiO_2 at 7 and 28 days. In this figure it is also possible to identify the two main peaks obtained in Fig. 4, confirming that the major hydrated phases present in this type of material are $Mg(OH)_2$ and M-S-H gel. From the TG analysis of Zhang et al. [23], where until 14 days the principal mass loss was observed below 300°C, it was noted that an increase in water content means a higher M-S-H gel content since a higher amount of water yielded a higher XRD intensity of the broad M-S-H features. Also, from DTG analysis in Fig. 5 it is observed that the curves do not return to a zero rate of mass loss after the first peak, suggesting that another decomposition process is taking place at the same time. This is also displayed in Fig. 4, where the M-S-H TG curve undergoes a progressive mass loss with lower slope from 235°C until nearly 700°C. This mass loss in M-S-H has been attributed to progressive dehydroxylation of disordered M-S-H, which has a range of hydroxyl environments [42]. This ongoing process is also noticeable in the temperature range above $Mg(OH)_2$ decomposition, where the DTG curve does not return to the values prior to the second peak.

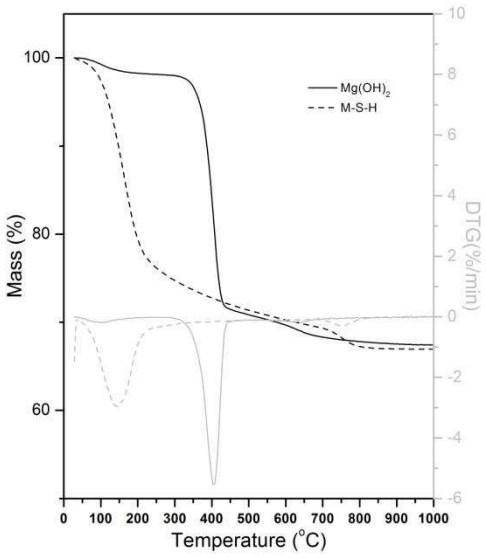

Fig. 4- TG and DTG traces for the hydrated MgO (AR200), and synthetic M-S-H gel with a 0.5 Mg/Si ratio.

To quantify the amounts of the different hydrated phases in the paste, DTG peaks were deconvoluted to identify the different decomposition processes, according to Fig. 1. The mass loss associated with the removal of water from the gel corresponds to the first peak centered at around 110-135°C. Based on Fig. 4, it is reasonable to delimit the dehydroxylation of $Mg(OH)_2$ (Equation 1) [35] in the range of temperatures between 330°C and 460°C:

$$Mg(OH)_2 \longrightarrow MgO + H_2O \quad (1)$$

Thus, a valid estimation of the amount of $Mg(OH)_2$ present in the samples is achieved by considering the deconvoluted mass loss in the second DTG peak. The loss of (OH^-) groups from the M-S-H gel can be quantified as the area of the curve centered at 460 °C in Fig. 1, that also comprises part of the second peak in Fig. 4. The results of mass loss displayed in Table 4 are obtained by deconvoluting the DTG curves, and the quantification of $Mg(OH)_2$ is in very good agreement with the XRD results (Table 3), so from these results it is confirmed that the formulation with higher content of MgO forms more $Mg(OH)_2$ at both 7 and 28 days. This amount of $Mg(OH)_2$ does not increase from 7 to 28 days since $Mg(OH)_2$ reacts with SiO_2 to form more M-S-H gel over time. Conversely to the $Mg(OH)_2$ results, the content of M-S-H decreases with increasing content of MgO at 7 days. However, at 28 days, the mass loss from magnesium silicate hydrate is always greater than at 7 days in each sample, achieving the highest mass loss in the 60% MgO – 40% SiO_2 system.

This is a preprint version of an article published in Materials & Design. The version of record is available at http://dx.doi.org/10.1016/j.matdes.2016.05.064

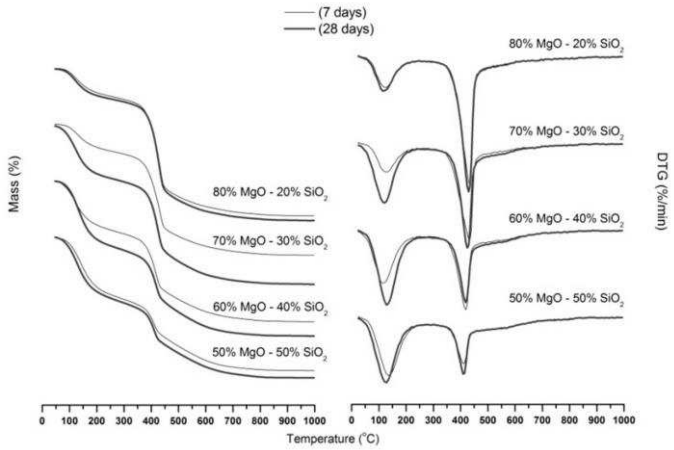

Fig. 5- TG (left) and DTG (rigth) graphs of the of the different MgO-SIO$_2$ samples at 7 days and at 28 days.

Table 4- Weight loss according to TG results of the different MgO-SiO$_2$ samples at different temperatures ranges.

		Mass loss (% of original)				
Formulation	Curing time	Total mass loss 50-1000°C	M-S-H dehydration	$Mg(OH)_2$ dehydroxilation	M-S-H dehydroxilation	$Mg(OH)_2$ (wt. %)
50%MgO-50%SiO_2	7 days	24,09	12,50	5,71	5,88	18,50
	28 days	24,76	13,47	4,95	6,34	16,04
60%MgO-40%SiO_2	7 days	25,06	9,43	8,22	7,41	26,62
	28 days	27,65	11,95	6,30	9,39	20,41
70%MgO-30%SiO_2	7 days	24,97	5,76	9,82	9,39	31,81
	28 days	28,28	9,98	10,46	7,84	33,87
80%MgO-20%SiO_2	7 days	26,01	5,85	13,30	6,86	43,08
	28 days	26,43	4,88	14,22	7,33	46,05

3.3 FT-IR characterization

The FT-IR results in Fig. 6a show that the systems containing MgO and SiO_2 present a similar FT-IR spectra to systems with 100% hydrated MgO, proving the significant influence of the $Mg(OH)_2$ structure in the hydrated pastes. Brucite is the main product expected from hydration of a powder with 97.4% MgO purity, and is a member of the group of minerals known as the layered hydroxides, whose structures show similarities to the layer and chain silicates as well as the basic building unit of all the layered double hydroxide (LDH) structure minerals [43]. Thus, it is not straightforward to establish which vibrational bands belong to $Mg(OH)_2$ and which to M-S-H gel. The 100% MgO hydrated sample shows bands around between 3000-3700, 1600, 1400 and 1040 cm^{-1} that are also present in the synthetic MgO-SiO_2 sample. For the 100% MgO sample the broadening peak from 3300 to 3600 cm^{-1} and the peak at 1600 cm^{-1} are derived from H-bonding of coordinated water [34,37] due to an excess of adsorbed water molecules on the $Mg(OH)_2$ surface, as the 0.5 w/c ratio exceeds the water requirement for MgO hydration. The sharp absorbance near 3696 cm^{-1} is a characteristic Mg–

OH stretch and around 1400 and 1040 cm^{-1} the Mg-OH bend is also evident [32,45,46]. In the literature the peak at 1040 cm^{-1} also reveals Si–O–Si vibrations of the tetrahedral sheets within the talc structure [21,38], and symmetrical stretching vibrations in M-S-H [21,33,38]. In previous works with M-S-H gels, identical bands are present at 1640 cm^{-1} [34] and 1400 cm^{-1} [29], as well as at 1040 cm^{-1}, hindering the identification of the phases by this technique.

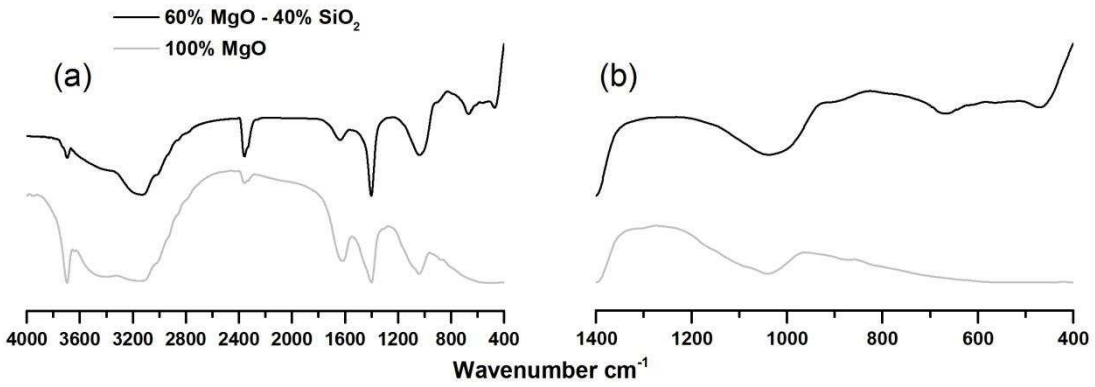

Fig. 6- FT-IR spectra of the 60 %MgO-40% SiO_2 and 100% MgO samples at 28 days in the region between 400-4000 cm^{-1} (a) and 1400-400 cm^{-1} (b).

Despite all the similarities in the spectra from 1000-4000 cm^{-1}, clear differences arise from 400 to 1000 cm^{-1} between the 100% MgO and the MgO-SiO_2 systems. For the MgO-SiO_2 systems, a sharp peak around 672 cm^{-1} arises due to Si–O bending vibrations [37,42] while Mg–O vibrations occur at 455 cm^{-1} [29,34]. After all the considerations, the FTIR results obtained in this study, it is possible to conclude that there is a reasonable similarity to the structure of different types magnesium silicate structures, such as treated talc, chrysotile and antigorite, as previously found in previous work were reaction of $Mg(OH)_2$ and SiO_2 was studied [21].

3.4 Hydration reactions and system compositions

On the basis of all the analysis carried out to understand the hydration of these cementitious systems, the stoichiometries of the different hydration reactions are presented in Table 5, representing the processes taking place at ages of 7 days and 28 days in each of the MgO-SiO_2 systems respectively:

This is a preprint version of an article published in Materials & Design. The version of record is available at http://dx.doi.org/10.1016/j.matdes.2016.05.064

Table 5- Calculated stoichiometry of the hydration reactions of the different formulations studied at 7 and 28 days, according to their molar proportions.

	7 days						
	MgO	SiO_2	H_2O	→		M-S-H gel	$Mg(OH)_2$
50% MgO-50% SiO_2	0.63	0.46	1.34	→	0.46	$Mg_{0.69}Si_1O_{2.69}(OH)_{0.71} \cdot 1.51H_2O$	0,32
60% MgO-40% SiO_2	0.83	0.39	1.39	→	0.39	$Mg_{0.97}Si_1O_{2.97}(OH)_{1.06} \cdot 1.35H_2O$	0,46
70% MgO-30% SiO_2	0.94	0.27	1.39	→	0.27	$Mg_{1.44}Si_1O_{3.44}(OH)_{1.92} \cdot 1.18H_2O$	0,55
80% MgO-20% SiO_2	1.02	0.15	1.45	→	0.15	$Mg_{1.87}Si_1O_{3.87}(OH)_{2.54} \cdot 2.17H_2O$	0,74
	28 days						
	MgO	SiO_2	H_2O	→		M-S-H gel	$Mg(OH)_2$
50% MgO-50% SiO_2	0.75	0.46	1.38	→	0.46	$Mg_{1.03}Si_1O_{2.87}(OH)_{0.77} \cdot 1.63H_2O$	0.28
60% MgO-40% SiO_2	0.85	0.40	1.54	→	0.40	$Mg_{1.25}Si_1O_{3.39}(OH)_{1.30} \cdot 1.65H_2O$	0.35
70% MgO-30% SiO_2	0.99	0.24	1.57	→	0.24	$Mg_{1.67}Si_1O_{3.55}(OH)_{1.79} \cdot 2.28H_2O$	0.58
80% MgO-20% SiO_2	1.06	0.09	1.47	→	0.09	$Mg_{2.82}Si_1O_{5.05}(OH)_{4.29} \cdot 2.86H_2O$	0.79

In Table 5, the columns labelled MgO, SiO_2 and H_2O represent the raw materials mixed, after correcting the molarity according to the purity of the powders and after subtracting the unreacted products after hydration. $Mg(OH)_2$ and unreacted MgO were determined as described before. Unreacted silica and water have been calculated as the difference between the original concentrations of raw materials and the concentrations in the M-S-H gel and $Mg(OH)_2$ produced. The H_2O and OH^- in M-S-H have been quantified from DTG analysis, and Mg in M-S-H has been estimated as the difference between the original concentration before mixing and the MgO present in $Mg(OH)_2$ and in unreacted MgO. With the help of EDS analysis (Table 6; see discussion below), Mg/Si was determined in the M-S-H particles so it was also possible to determine the Si content in M-S-H. It is important to remark that the excess H_2O, beyond the stoichiometric quantities required for reaction, was required for proper mixing and good workability to mold the samples. This excess water is evaporated in the drying process, generating voids in the matrix. Fig. 7 displays the mass fraction distribution at 7 and 28 days, calculated from Table 5.

This is a preprint version of an article published in Materials & Design. The version of record is available at http://dx.doi.org/10.1016/j.matdes.2016.05.064

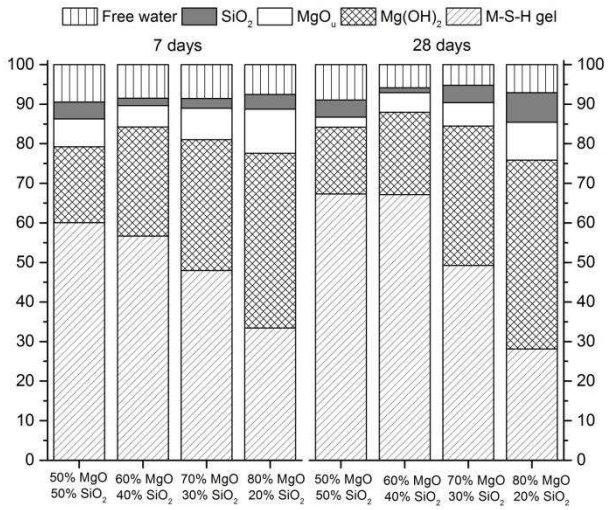

Fig. 7- Mass fraction distribution of all the components of MgO-SiO_2 pastes, determined from the analytical results. MgO_u is unreacted precursor MgO.

3.5 SEM

A micrograph of a polished surface of the 28-day hydrated paste of the 60% MgO-40% SiO_2 system is shown in Fig. 8(a). The microstructure is mainly comprised of $Mg(OH)_2$ crystals dispersed in an M-S-H gel matrix. The $Mg(OH)_2$ particles present two equal-dimensioned axes with clearly defined corners. In Fig. 8(b), the same image as in Fig. 8(a) is edited with the help of EDS mapping to identify the different phases in the cement. The brucite particles have been thresholded in greenish yellow, and the regions in blue are the M-S-H gel. Small white particles correspond to unreacted silica. Darker blue zones match the impurities present in the MgO powder.

Table 6- Mg/Si ratio for the different MgO-SiO_2 systems according EDS results.

Age		50% MgO 50% SiO_2		60% MgO 40% SiO_2		70% MgO 30% SiO_2		80% MgO 20% SiO_2	
		Mg/Si	MgO/SiO_2	Mg/Si	MgO/SiO_2	Mg/Si	MgO/SiO_2	Mg/Si	MgO/SiO_2
7 days	$\bar{x}$	**0.69**	**0.48**	**0.97**	**0.64**	**1.44**	**1.00**	**1.87**	**1.18**
	σ	0.07	0.03	0.07	0.03	0.17	0.08	0.08	0.08
28 days	$\bar{x}$	**1.03**	**0.69**	**1.25**	**0.81**	**1.67**	**1.12**	**2.82**	**1.82**
	σ	0.05	0.03	0.17	0.10	0.15	0.10	0.29	0.10

$\bar{x}$ stands for average values and σ stands for standard deviation

The interface between $Mg(OH)_2$ crystals and M-S-H gel has also been highlighted in grey. Using EDS mapping it is possible to establish that the interface has a high concentration of Si atoms. Considering the $Mg(OH)_2$ crystals as a region of almost zero Si concentration, on the boundaries of these particles an overconcentration of unreacted silica is produced.

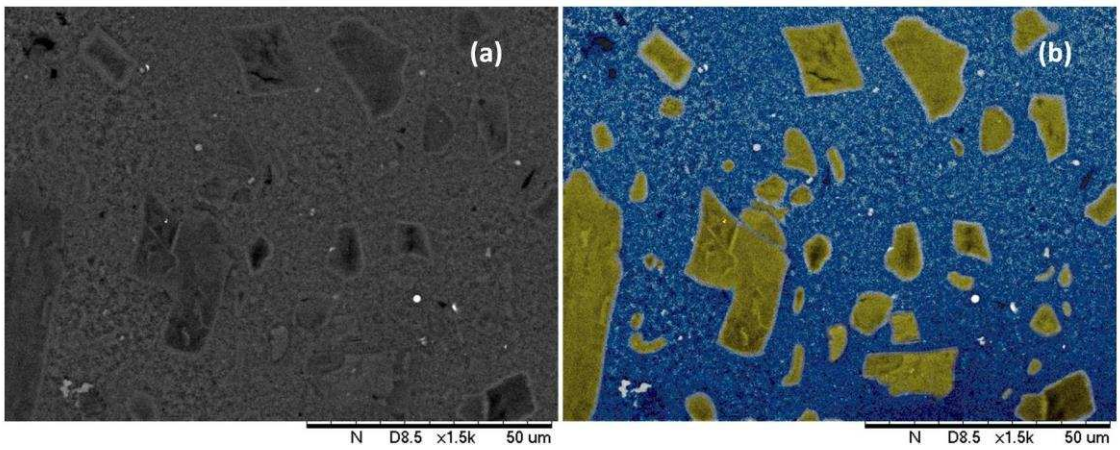

Fig. 8 (a) SEM image of the polished surface of a 60% MgO – 40% SiO_2 paste at 28 days. (b) False-color version of the SEM image in (a); greenish yellow particles are $Mg(OH)_2$, blue regions are M-S-H gels and white particles are unreacted SiO_2.

According to the reaction mechanism for hydration of MgO [46,47], water is chemisorbed on MgO to form a liquid layer on the surface. The water then reacts with the MgO to form a surface layer of $Mg(OH)_2$, which subsequently dissolves into the water layer and, only after this layer becomes saturated, precipitation takes place. As significant quantities of OH^- anions are released, SiO_2 dissolves to form silicic acid ($Si(OH)_4$ and deprotonated anionic forms $\equiv Si\text{-}O^-$) [48], which increase the concentration of Si surrounding $Mg(OH)_2$ crystals as seen in Figure 8. The presence of Mg^{2+} cations balances the charges of these anions, and the apparition of the $–Si–O–Mg^{2+}$ linkage does not allow the reverse reaction to form siloxane bonds. For longer curing times, the TG curves tend to be smoother, indicating a more continuous transition from brucite to M–S–H in the region between 300 and 550°C. Also, from the TG curves in which synthetic gels have been used [28,37] it can be deduced that in this range of temperatures (300-550°C) gel dehydroxylation takes place, suggesting that the OH^- ions from $Mg(OH)_2$ become a part of the poorly-crystallized structure of the magnesium silicate hydrates, potentially associated with defects in the silicate structures in the layered structure.

3.6 Matrix selection for fiber-cement purposes: pH evaluation and compressive strength analysis

From Fig. 9 it can be seen that all the samples containing MgO present notably lower pH values than the CPV-ARI (High Early Strength Portland Cement) samples, confirming a lower concentration of OH^- ions in the pore solution associated with the matrix. While the Control sample keeps stable pH values with time (12.8-13.0), the MgO-containing samples present a descending trend in pH with time, for all the formulations. As MgO content is increased in the MgO-SiO_2 formulations, the pH values do not decrease as much as for samples with lower contents of MgO. The most important reduction in pH occurs between 1 and 7 days. From that

age onwards, only the 50% MgO – 50% SiO_2 samples present a continuous pH decrease until the age of 21 days, when it stabilizes. The pH results here are consistent with previous works where MgO-SiO_2 systems were analyzed [20], obtaining pH values below 10 at 28 days. The samples containing 60% MgO and 40% SiO_2 have a pH value around 10 at 7 days, decreasing with time to reach a pH value of 9.8. This reduced alkalinity could be very advantageous since pH values below 11 at early age help to prevent cellulosic fiber degradation in fiber-reinforced composites [14].

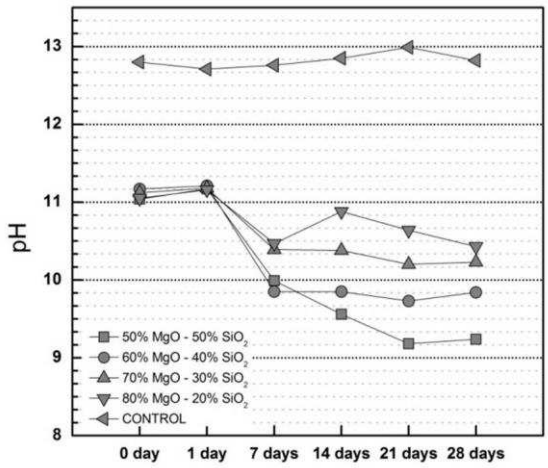

Fig. 9- pH evolution over time of different MgO-SiO_2 blended systems and control samples (100% Portland cement).

Fig. 10 shows the compressive strength results. At 7 days, there is a slight enhancement of the mechanical strength with the increase of the MgO in the samples. This difference is statistically significant (Table 7) when the MgO content varies from 60 to 70%, but at 7 days of curing the samples containing 50 and 60% of MgO and those with 70 and 80% each have statistically similar values. At this same age, Control samples have significantly higher strengths compared to almost every sample with MgO. The only sample with an equivalent performance is 80% MgO – 20% SiO_2.

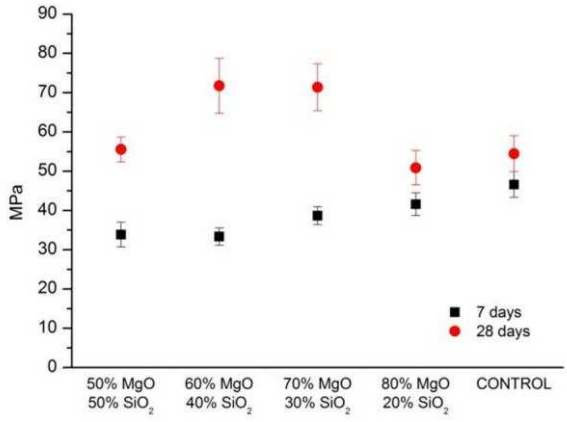

Fig. 10- Axial compressive strength of different MgO-SiO_2 pastes and control samples (100% Portland cement) at 7 and 28 days.

However, at 28 days, all the formulations containing MgO have at least equivalent strength to the control samples. It is also remarkable that the MgO-SiO_2 samples present a strength improvement from 7 to 28 days for every formulation, in contrast to the control samples which have no statistically considerable variation. The 60% MgO – 40% SiO_2 and 70% MgO – 30% SiO_2 systems have the highest strengths, 71.8 and 71.4 MPa respectively, showing a statistical difference from the rest of the samples. These values are also around 30% higher than the control samples, which have an average compressive strength of 54.5 MPa. This fact may be explained because of the rather high water to cement ratio (0.50) used to mold the Portland cement pastes, for consistency with the water contents of the MgO-SiO_2 systems. A w/c value of 0.50 is not disproportionate for MgO-SiO_2 systems, according to Lothenbach et al. [37], who established that M-S-H gels present a silicate sheet structure and a higher amount of chemically bound water compared to Portland cement.

Table 7- Compressive strength results of the different MgO-SiO_2 systems and Control samples (100% Portland cement). Tukey tests (0.05 confidence) are represented next to the numerical values. The ratio of compressive strength at 28 days to compressive strength at 7 days is in the right-most column.

		7d	28d	R_{c28d}/R_{c7d}
50% MgO 50% SiO_2	$\bar{x}$ (MPa)	**33.9 a, A**	**55.5 a, B**	**1.64**
	σ (MPa)	3.15	3.13	
60% MgO 40% SiO_2	$\bar{x}$ (MPa)	**33.4 a, A**	**71.8 b, B**	**2.15**
	σ (MPa)	2.20	7.00	
70% MgO 30% SiO_2	$\bar{x}$ (MPa)	**38.7 a, b, A**	**71.4 b, B**	**1.85**
	σ (MPa)	2.27	6.00	
80% MgO 20% SiO_2	$\bar{x}$ (MPa)	**41.6 b, c, A**	**50.9 a, B**	**1.22**
	σ (MPa)	2.90	4.38	
CONTROL	$\bar{x}$ (MPa)	**46.6 c, A**	**54.5 a, A**	**1.17**
	σ (MPa)	3.29	4.57	

Same lower case letters in the same column mean no statistically significant difference.
Same capital letters in the same row mean no statistically significant difference.
$\bar{x}$ stands for mean values and σ is standard deviation.

Considering the results presented in Fig. 11, it is reasonable to establish a relationship between compressive strength, and both free water and the total amount of hydrated phases in the systems. A lower free water content in the matrix leads to higher compressive strength at 7 days. Another key aspect is the influence of $Mg(OH)_2$ on the strength at early stages, since mechanical performance at 7 days is statistically superior for samples with higher brucite content.

This is in line with what happens with other types of inorganic cement, such as Portland cement [49,50], where an increase of porosity leads to a drastic decrease of mechanical properties. This relation is based on the reduction of the capillary porosity, which helps to reduce the Gel-Space Ratio (GSR) of any cement [51]. In the case of MgO-SiO_2 samples, there is

a correlation at 28 days between compressive strength and unreacted water at 28 days as described by equation 2:

$$G_W SR = \frac{V_{Gw}}{V_{Gw}+W_u} \qquad (2)$$

where $G_w SR$ is defined as the Water Gel Space Ratio, V_{Gw} is the volume of the water from M-S-H gel and W_u is the volume of the unreacted water (excess from mixing water that is neither in M-S-H nor in $Mg(OH)_2$). Thus it can be proved that, even after 28 days, the presence of $Mg(OH)_2$ is important to reduce the amount of free water and thus to create a denser matrix. This provides interesting evidence which enables the conclusion that the amount of M-S-H is not the only determining factor which must be considered in designing cements with higher strength in the initial stages of reaction.

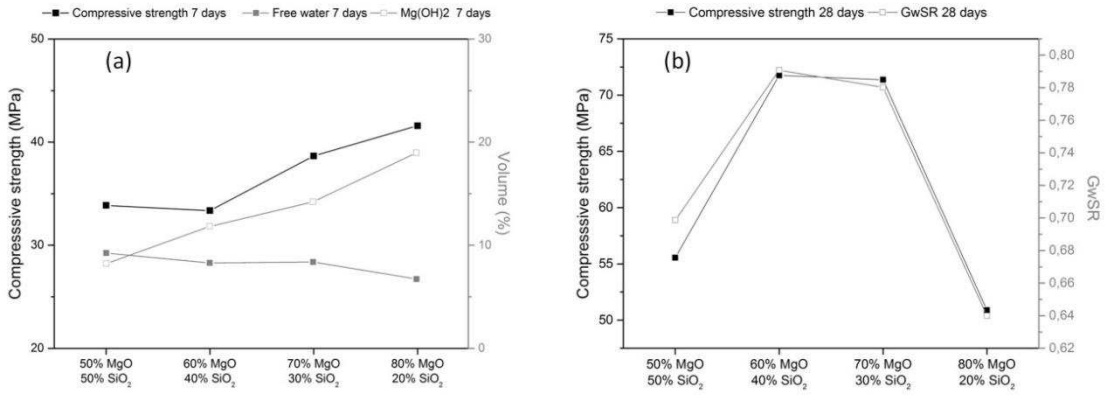

Fig. 11. (a) Trends in the compressive axial strength (left axis) and free water and brucite content (right axis). (b) Trends in the compressive strength (left axis) and GwSR (right axis).

Paying closer attention to the relationship between compressive strength and the MgO/SiO_2 ratio for the different formulations (Fig. 12), at 7 days it is possible to detect how the higher MgO/SiO_2 ratio yields a higher compressive strength. However this trend is not displayed at 28 days, where the formulation with highest MgO/SiO_2 ratio (80% MgO – 20% SiO_2) presents the lowest mechanical performance. All that can be deduced from Fig. 12 is that the formulations with the uppermost strength for both ages, 7 and 28 days, present MgO/SiO_2 ratios ranging from 0.8-1.2, in agreement with what was noted in the literature [21,37,38,52]. This difference in Mg/Si content may be associated to a change in M-S-H gel structure [21,29,37], achieving a more resistant structure (Q^3 silica tetrahedra) for MgO/SiO_2 ratios around 0.8-1.2. However, the key correlation which determines strength evidently involves the GSR, rather than the strength being dominated by the Mg/Si ratio in the gel.

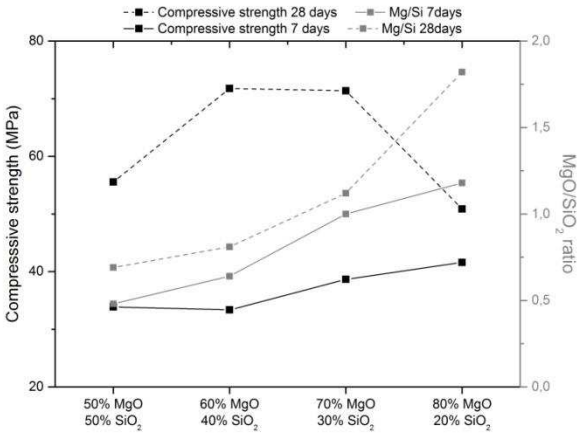

Fig. 12- Trends in the compressive strength (left axis) and Mg/Si ratio (right axis).

In view of the pH and compressive strength results, in order to choose the optimal matrix to produce fiber-cement products reinforced with lignocellulosic fibers, the system that would offer the lowest pH value is the 50% MgO – 50% SiO_2 formulation. However this formulation has approximately 30% less compressive strength compared with the 60% MgO – 40% SiO_2 formulation, and the difference in pH between these two formulations is in any case not very noteworthy. The most promising formulation thus selected is the 60-40 blend, since it is the one that offers the better compromise between alkalinity and mechanical properties, compared to the 50-50 and 70-30 formulations.

3.7 Fiber-cement bending tests

Based on the flexural results (Table 8), the best strength results at 28 days are obtained by the control samples. This may be because the water to cement ratio needed in the MgO-SiO_2 samples to enable the fiber-cement molding process was greater than the value of 0.50 which was used to produce samples for compression tests. However, after 200 accelerated aging cycles, the control samples suffer a significant loss of flexural strength as has been demonstrated by other authors [9,53], whereas the optimized MgO-SiO_2 formulation increases in modulus of rupture (MOR). This suggests that the hydration reactions of MgO-SiO_2 system continue beyond 28 days of age, in accordance with the findings of other researchers [38,27]. However the test data that best show the efficiency of this type of cement for the preservation of the capacity of the reinforcing fibers is the specific deflection at MOR. Samples with 60% MgO – 40% SiO_2, even at 28 days, have higher specific deflection values than the control samples. After accelerated aging, the MgO-SiO_2 samples maintain approximately 90% of the specific deformation in the MOR. This small loss of ductility, although potentially not statistically significant, can be explained by the modification of the fiber-matrix interface,

which becomes more densified as a consequence of the matrix hydration over time [12]. This induces modification of the mechanical behavior of the composite, becoming more rigid. In light of these flexural tests, it is evident that the binder system developed here offers better performance in terms of durability compared to Portland cement when fiber-cement products reinforced with cellulosic fibers are conceived.

Table 8- Flexural results of the fiber-cement specimens at 28 days and after 200 cycles of accelerated ageing (200 aac) for samples made using MgO-SiO_2 and Portland (control) cements.

	MOR (MPa)				SD at MOR (mm/mm)			
	28 days		200 aac		28 days		200 aac	
	$\bar{x}$	σ	$\bar{x}$	σ	$\bar{x}$	σ	$\bar{x}$	σ
60% MgO – 40% SiO_2	9.21a, A	0.48	10.63a, B	0.35	0.021a, A	0.005	0.019a, A	0.005
Control	9.82b, A	0.25	6.23b, B	0.78	0.012b, A	0.005	0.003b, B	0.001

Same lower case letters in the same column mean no statistical significant difference.
Same capital letters in the same row mean no significant statistical significant difference.
$\bar{x}$ stands for average values and σ stands for standard deviation.

4. CONCLUSIONS

In systems where MgO and SiO_2 are mixed with water, the hydration products obtained are $Mg(OH)_2$ and M-S-H gels for all the formulations studied, regardless of age (7 and 28 days). From TG tests on samples 100% $Mg(OH)_2$ and M-S-H gels, it is possible to determine the amount of $Mg(OH)_2$ in the blended samples, via the mass loss observed between 300 and 550^{o}C. For formulations with higher MgO content, a higher content of $Mg(OH)_2$ is obtained as hydration product.

The M-S-H gels obtained both at 7 and 28 days have an Mg/Si ratio which increases with increasing MgO content. Similarly, for all samples the Mg/Si ratio increases over time, which can be interpreted as a change in the gel structure over time because the reaction is still not complete after 28 days. SEM micrographs show that particles of $Mg(OH)_2$ are surrounded by areas of high concentration of Si, which is interpreted as a region where there has been notable dissolution of SiO_2 to form $Si(OH)_4$. This in turn facilitates the dissociation of Mg^{2+} and OH^-, promoting the formation of laminar structures of silicates which subsequently form part of the structure of the M-S-H gels.

Maximizing the content of M-S-H gel does not necessarily increase mechanical performance of the samples. Conversely, at 7 days there is a correlation between the content of $Mg(OH)_2$ and the compressive strength of the samples, indicating that the mechanical properties are not influenced exclusively by the M-S-H gel content. This is corroborated even at 28 days where the formulation with highest mechanical strength is again not the one with a highest M-S-H gel content. There seems to be a clear link between the amount of pores associated with the free

water present in the matrix after the hydration reactions, and the compressive strength, which is well described by the Gel-Space Ratio concept, and this parameter correlates closely with compressive strength.

Samples with less MgO content have lower pH values. The formulations 60% MgO-40% SiO_2 and 70% MgO-30% SiO_2 have the highest compressive strength values at 28 days, with no statistical difference. For this reason, the mix with 60% MgO-40% SiO_2 is chosen as optimal for the development of fiber-cement composites, since it is the most mechanically resistant and is less alkaline compared with 70% MgO-30% SiO_2. The efficiency of the MgO-SiO_2-H_2O system for the preservation of the reinforcing capacity of the cellulosic has been proved by application of a 4 point bending test at 28 days and after 200 cycles of accelerated aging. After aging, samples produced with 60% MgO-40% SiO_2 and cellulosic fiber reinforcement show no statistically significant reduction in Modulus of Rupture (MOR), and no change in deformation at the point of rupture, in contrast to samples produced with Portland cement, where both properties drastically decay.

5. ACKNOWLEDGMENTS

The authors acknowledge the Brazilian financial support from Fundação de Amparo à Pesquisa do Estado de São Paulo (FAPESP Thematic Project, Grant n: 2012/51467-3). The authors thank Andzej Rudzis for his help with image mapping. We also thank Magnesita Refratários S.A. and Elkem Materials South América for providing the materials for the cement production.

REFERENCES

[1] M. Ardanuy, J. Claramunt, R.D. Toledo Filho, Cellulosic fiber reinforced cement-based composites: A review of recent research, Constr. Build. Mater. 79 (2015) 115–128. doi:10.1016/j.conbuildmat.2015.01.035.

[2] F.J. Baeza, O. Galao, E. Zornoza, P. Garcés, Effect of aspect ratio on strain sensing capacity of carbon fiber reinforced cement composites, Mater. Des. 51 (2013) 1085–1094. doi:10.1016/j.matdes.2013.05.010.

[3] X. Shu, R.K. Graham, B. Huang, E.G. Burdette, Hybrid effects of carbon fibers on mechanical properties of Portland cement mortar, Mater. Des. 65 (2015) 1222–1228. doi:10.1016/j.matdes.2014.10.015.

[4] T.-Y. Han, W.-T. Lin, A. Cheng, R. Huang, C.-C. Huang, Influence of polyolefin fibers on the engineering properties of cement-based composites containing silica fume, Mater. Des. 37 (2012) 569–576. doi:10.1016/j.matdes.2011.10.038.

[5] T. Gupta, S. Chaudhary, R.K. Sharma, Mechanical and durability properties of waste rubber fiber concrete with and without silica fume, J. Clean. Prod. 112 (2016) 702–711. doi:10.1016/j.jclepro.2015.07.081.

[6] P. Asokan, M. Osmani, A.D.F. Price, Assessing the recycling potential of glass fibre reinforced plastic waste in concrete and cement composites, J. Clean. Prod. 17 (2009) 821–829. doi:10.1016/j.jclepro.2008.12.004.

[7] R. Madandoust, M.M. Ranjbar, R. Ghavidel, S. Fatemeh Shahabi, Assessment of factors influencing mechanical properties of steel fiber reinforced self-compacting concrete, Mater. Des. 83 (2015) 284–294. doi:10.1016/j.matdes.2015.06.024.

[8] S. Senaratne, D. Gerace, O. Mirza, V.W.Y. Tam, W.-H. Kang, The costs and benefits of combining recycled aggregate with steel fibres as a sustainable, structural material, J. Clean. Prod. 112 (2016) 2318–2327. doi:10.1016/j.jclepro.2015.10.041.

[9] J. de A. Melo Filho, F. de A. Silva, R.D. Toledo Filho, Degradation kinetics and aging mechanisms on sisal fiber cement composite systems, Cem. Concr. Compos. 40 (2013) 30–39. doi:10.1016/j.cemconcomp.2013.04.003.

[10] R.D. Toledo Filho, F. de A. Silva, E.M.R. Fairbairn, J. de A.M. Filho, Durability of compression molded sisal fiber reinforced mortar laminates, Constr. Build. Mater. 23 (2009) 2409–2420. doi:10.1016/j.conbuildmat.2008.10.012.

[11] J. Wei, C. Meyer, Improving degradation resistance of sisal fiber in concrete through fiber surface treatment, Appl. Surf. Sci. 289 (2014) 511–523. doi:10.1016/j.apsusc.2013.11.024.

[12] R.D. Toledo Filho, K. Scrivener, G.L. England, K. Ghavami, Durability of alkali-sensitive sisal and coconut fibres in cement mortar composites, Cem. Concr. Compos. 22 (2000) 127–143. doi:10.1016/S0958-9465(99)00039-6.

[13] C.L. Pereira, H. Savastano Jr., J. Payá, S.F. Santos, M.V. Borrachero, J. Monzó, L. Soriano, Use of highly reactive rice husk ash in the production of cement matrix reinforced with green coconut fiber, Ind. Crops Prod. 49 (2013) 88–96. doi:10.1016/j.indcrop.2013.04.038.

[14] G. Mármol, S.F. Santos, H. Savastano Jr., M.V. Borrachero, J. Monzó, J. Payá, Mechanical and physical performance of low alkalinity cementitious composites reinforced with recycled cellulosic fibres pulp from cement kraft bags, Ind. Crops Prod. 49 (2013) 422–427. doi:10.1016/j.indcrop.2013.04.051.

[15] E.M. Bezerra, A.P. Joaquim, H. Savastano, V.M. John, V. Agopyan, The effect of different mineral additions and synthetic fiber contents on properties of cement based composites, Cem. Concr. Compos. 28 (2006) 555–563. doi:10.1016/j.cemconcomp.2006.02.001.

[16] A.E.F.S. Almeida, G.H.D. Tonoli, S.F. Santos, H. Savastano Jr., Improved durability of vegetable fiber reinforced cement composite subject to accelerated carbonation at early age, Cem. Concr. Compos. 42 (2013) 49–58. doi:10.1016/j.cemconcomp.2013.05.001.

[17] S.F. Santos, R. Schmidt, A.E.F.S. Almeida, G.H.D. Tonoli, H. Savastano, Supercritical carbonation treatment on extruded fibre–cement reinforced with vegetable fibres, Cem. Concr. Compos. 56 (2015) 84–94. doi:10.1016/j.cemconcomp.2014.11.007.

[18] V.D. Pizzol, L.M. Mendes, H. Savastano, M. Frías, F.J. Davila, M.A. Cincotto, V.M. John, G.H.D. Tonoli, Mineralogical and microstructural changes promoted by accelerated carbonation and ageing cycles of hybrid fiber–cement composites, Constr. Build. Mater. 68 (2014) 750–756. doi:10.1016/j.conbuildmat.2014.06.055.

[19] B. Sandberg, T. Mosberg, Ceramic Transactions. Advances in refractories technology, American Ceramic Society, Westerville, Ohio, 1989.

[20] T. Zhang, C.R. Cheeseman, L.J. Vandeperre, Development of low pH cement systems forming magnesium silicate hydrate (M-S-H), Cem. Concr. Res. 41 (2011) 439–442. doi:10.1016/j.cemconres.2011.01.016.

[21] S.A. Walling, H. Kinoshita, S.A. Bernal, N.C. Collier, J.L. Provis, Structure and properties of binder gels formed in the system $Mg(OH)_2$–SiO_2–H_2O for immobilisation of Magnox sludge, Dalton Trans. 44 (2015) 8126–8137. doi:10.1039/C5DT00877H.

[22] W. Jiangxiong, C. Yimin, L. Yongxin, The reaction mechanism between MgO and microsilica at room temperature, J. Wuhan Univ. Technol.-Mater. Sci. 21 (2006) 88–91.

[23] T. Zhang, L.J. Vandeperre, C.R. Cheeseman, Formation of magnesium silicate hydrate (M-S-H) cement pastes using sodium hexametaphosphate, Cem. Concr. Res. 65 (2014) 8–14. doi:10.1016/j.cemconres.2014.07.001.

[24] S.F. Santos, G.H.D. Tonoli, J.E.B. Mejia, J. Fiorelli, H. Savastano Jr, Compuestos cementantes no convencionales reforzados con fibras vegetales: Una revisión de estrategias para mejorar la durabilidad, Mater. Constr. 65 (2015) e041. doi:10.3989/mc.2015.05514.

[25] M.A. Shand, The chemistry and technology of magnesia, Wiley-Interscience, Hoboken, N.J, 2006.

[26] S.K. Antiohos, V.G. Papadakis, S. Tsimas, Rice husk ash (RHA) effectiveness in cement and concrete as a function of reactive silica and fineness, Cem. Concr. Res. 61–62 (2014) 20–27. doi:10.1016/j.cemconres.2014.04.001.

[27] J. Szczerba, R. Prorok, E. Śnieżek, D. Madej, K. Maślona, Influence of time and temperature on ageing and phases synthesis in the MgO–SiO2–H2O system, Thermochim. Acta. 567 (2013) 57–64. doi:10.1016/j.tca.2013.01.018.

[28] C. Roosz, S. Grangeon, P. Blanc, V. Montouillout, B. Lothenbach, P. Henocq, E. Giffaut, P. Vieillard, S. Gaboreau, Crystal structure of magnesium silicate hydrates (M-S-H): The relation with 2:1 Mg–Si phyllosilicates, Cem. Concr. Res. 73 (2015) 228–237. doi:10.1016/j.cemconres.2015.03.014.

[29] D.R.M. Brew, F.P. Glasser, Synthesis and characterisation of magnesium silicate hydrate gels, Cem. Concr. Res. 35 (2005) 85–98. doi:10.1016/j.cemconres.2004.06.022.

[30] J.E.M. Ballesteros, S.F. Santos, G. Mármol, H. Savastano, J. Fiorelli, Evaluation of cellulosic pulps treated by hornification as reinforcement of cementitious composites, Constr. Build. Mater. 100 (2015) 83–90. doi:10.1016/j.conbuildmat.2015.09.044.

[31] H. Savastano Jr., P.. Warden, R.S.. Coutts, Brazilian waste fibres as reinforcement for cement-based composites, Cem. Concr. Compos. 22 (2000) 379–384. doi:10.1016/S0958-9465(00)00034-2.

[32] EN 494:2012+A1:2015, Fibre-cement profiled sheets and fittings. Product specification and test methods, European Committee for Standarization, CEN-CENELEC Managment centre: Avenue Marnix 17, B-1000 Brussels, 2012.

[33] I. Rashid, N. Daraghmeh, M. Al-Remawi, S.A. Leharne, B.Z. Chowdhry, A. Badwan, Characterization of chitin-metal silicates as binding superdisintegrants, J. Pharm. Sci. 98 (2009) 4887–4901. doi:10.1002/jps.21781.

[34] I.M. Ali, Y.H. Kotp, I.M. El-Naggar, Thermal stability, structural modifications and ion exchange properties of magnesium silicate, Desalination. 259 (2010) 228–234. doi:10.1016/j.desal.2010.03.054.

[35] J. Temuujin, K. Okada, K.J.D. MacKenzie, Role of Water in the Mechanochemical Reactions of MgO–SiO2Systems, J. Solid State Chem. 138 (1998) 169–177. doi:10.1006/jssc.1998.7768.

[36] J. Temuujin, K. Okada, K.J.D. MacKenzie, Formation of Layered Magnesium Silicate during the Aging of Magnesium Hydroxide-Silica Mixtures, J. Am. Ceram. Soc. 81 (2005) 754–756. doi:10.1111/j.1151-2916.1998.tb02405.x.

[37] B. Lothenbach, D. Nied, E. L'Hôpital, G. Achiedo, A. Dauzères, Magnesium and calcium silicate hydrates, Cem. Concr. Res. 77 (2015) 60–68. doi:10.1016/j.cemconres.2015.06.007.

[38] F. Jin, A. Al-Tabbaa, Strength and hydration products of reactive MgO–silica pastes, Cem. Concr. Compos. 52 (2014) 27–33. doi:10.1016/j.cemconcomp.2014.04.003.

[39] J. Liao, M. Senna, Mechanochemical dehydration and amorphization of hydroxides of Ca, Mg and Al on grinding with and without SiO2, Solid State Ion. 66 (1993) 313–319. doi:10.1016/0167-2738(93)90421-X.

[40] T. Zhang, L.J. Vandeperre, C.R. Cheeseman, Formation of magnesium silicate hydrate (M-S-H) cement pastes using sodium hexametaphosphate, Cem. Concr. Res. 65 (2014) 8–14. doi:10.1016/j.cemconres.2014.07.001.
[41] V.S. Ramachandran, ed., Handbook of thermal analysis of construction materials, Noyes Publications/William Andrew Pub, Norwich, N.Y, 2003.
[42] D. Nied, K. Enemark-Rasmussen, E. L'Hopital, J. Skibsted, B. Lothenbach, Properties of magnesium silicate hydrates (M-S-H), Cem. Concr. Res. 79 (2016) 323–332. doi:10.1016/j.cemconres.2015.10.003.
[43] P.V. Kamath, G.H. Annal Therese, J. Gopalakrishnan, On the Existence of Hydrotalcite-Like Phases in the Absence of Trivalent Cations, J. Solid State Chem. 128 (1997) 38–41. doi:10.1006/jssc.1996.7144.
[44] P.S. Braterman, Vibrational spectroscopy of brucite: A molecular simulation investigation, Am. Mineral. 91 (2006) 1188–1196. doi:10.2138/am.2006.2094.
[45] R. Hanna, Infrared Properties of Magnesium Oxide, J. Am. Ceram. Soc. 48 (1965) 376–380. doi:10.1111/j.1151-2916.1965.tb14765.x.
[46] W. Feitknecht, H. Braun, Der Mechanismus der Hydratation von Magnesiumoxid mit Wasserdampf, Helv. Chim. Acta. 50 (1967) 2040–2053. doi:10.1002/hlca.19670500738.
[47] O. Fruhwirth, G.W. Herzog, I. Hollerer, A. Rachetti, Dissolution and hydration kinetics of MgO, Surf. Technol. 24 (1985) 301–317. doi:10.1016/0376-4583(85)90080-9.
[48] G.B. Alexander, W.M. Heston, R.K. Iler, The Solubility of Amorphous Silica in Water, J. Phys. Chem. 58 (1954) 453–455. doi:10.1021/j150516a002.
[49] F.M. Lea, P.C. Hewlett, Lea's chemistry of cement and concrete, (2004).
[50] H.F.W. Taylor, Cement chemistry, 2nd ed, T. Telford, London, 1997.
[51] P. Termkhajornkit, Q.H. Vu, R. Barbarulo, S. Daronnat, G. Chanvillard, Dependence of compressive strength on phase assemblage in cement pastes: Beyond gel–space ratio — Experimental evidence and micromechanical modeling, Cem. Concr. Res. 56 (2014) 1–11. doi:10.1016/j.cemconres.2013.10.007.
[52] Z. Li, T. Zhang, J. Hu, Y. Tang, Y. Niu, J. Wei, Q. Yu, Characterization of reaction products and reaction process of MgO–SiO2–H2O system at room temperature, Constr. Build. Mater. 61 (2014) 252–259. doi:10.1016/j.conbuildmat.2014.03.004.
[53] B.J. Mohr, J.J. Biernacki, K.E. Kurtis, Microstructural and chemical effects of wet/dry cycling on pulp fiber–cement composites, Cem. Concr. Res. 36 (2006) 1240–1251. doi:10.1016/j.cemconres.2006.03.020.